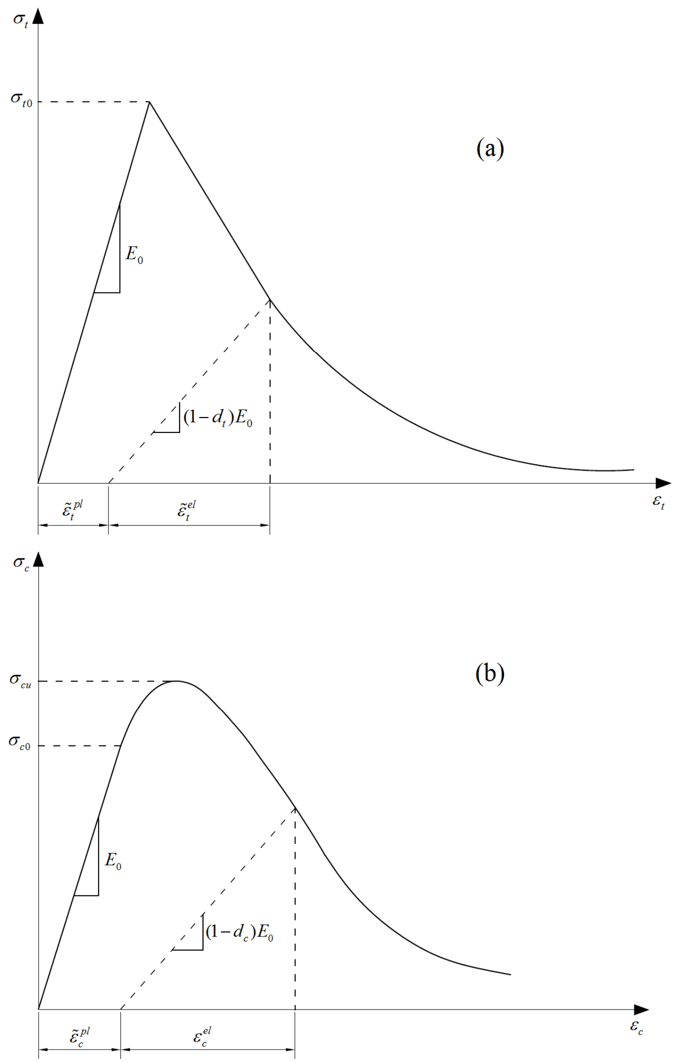

Figure 3—Response of concrete under uniaxial loading in tension (a) and compression (b).

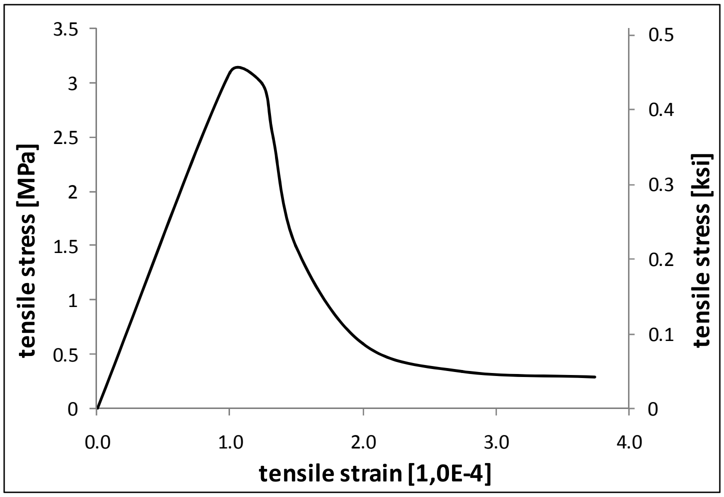

Figure 4—Tensile stress-strain curve for concrete.

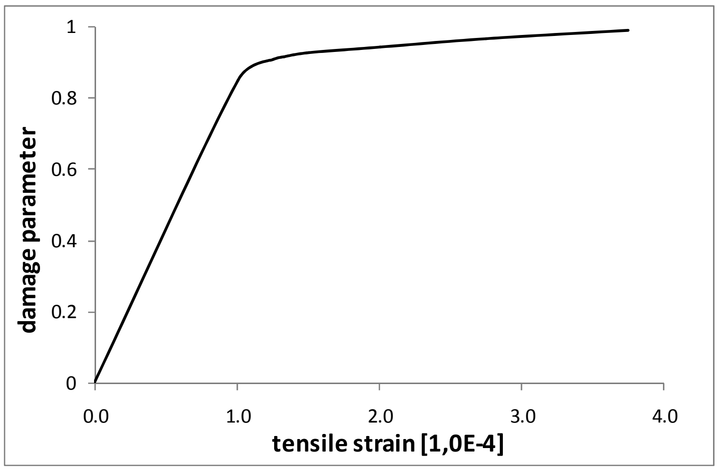

Figure 5—Tensile damage-stress curve for concrete.

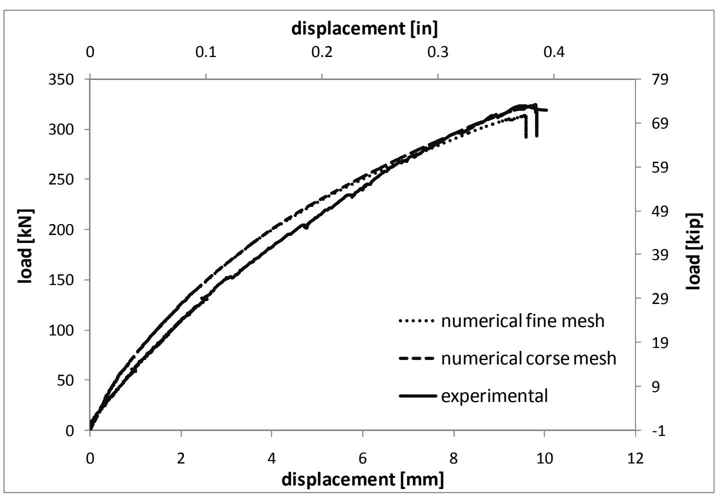

Figure 6—Load vs. displacement diagram for the beam without FRP reinforcement: experimental and numerical results (1 in. = 25.4 mm; 1ksi = 6.895 MPa).

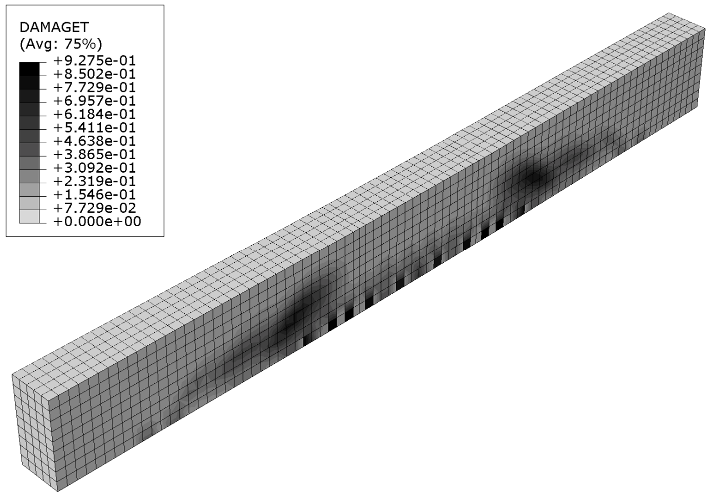

Figure 7—Contour of the tensile damage in the fine numerical model.

Figure 8—Experimental cracking pattern for the control beam (Pellegrino and Modena 2002).

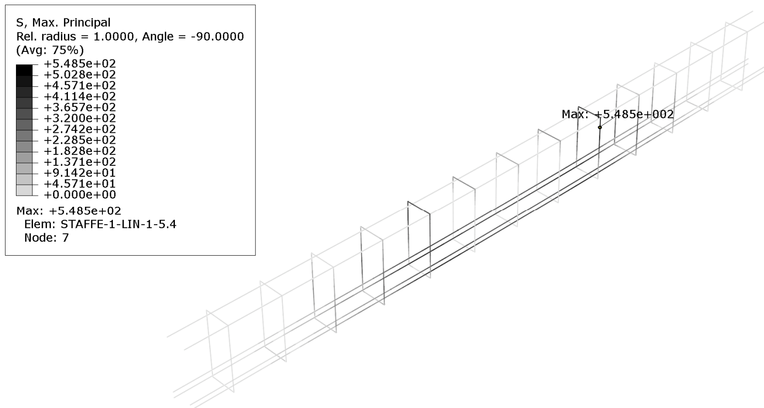

Figure 9—Contour of the normal stresses in the internal steel longitudinal bars and stirrups: the maximum value is achieved in node 7 of the stirrup intercepted by the main diagonal crack.

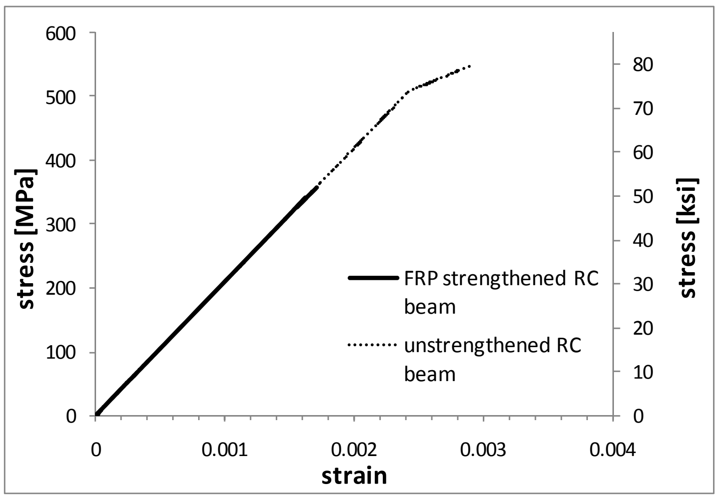

Figure 10—Stress-strain relationship for the node n7 of the stirrup intercepted by the main diagonal crack.

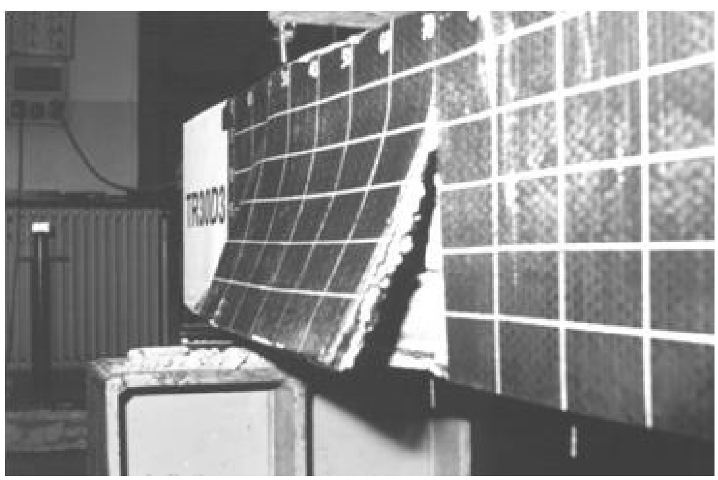

Figure 11—Peeling of the concrete cover in the FRP strengthened RC beam (Pellegrino and Modena 2002).

Figure 12—FRP strengthened RC beam after the removal of the peeled concrete cover (Pellegrino and Modena 2002).

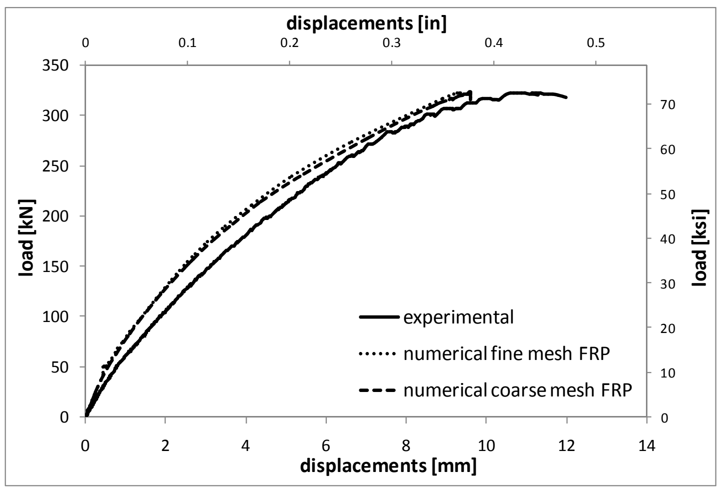

Figure 13— Load-displacement diagram for FRP strengthened RC beams, experimental and numerical results (1 in. = 25.4 mm; 1ksi = 6.895 MPa).

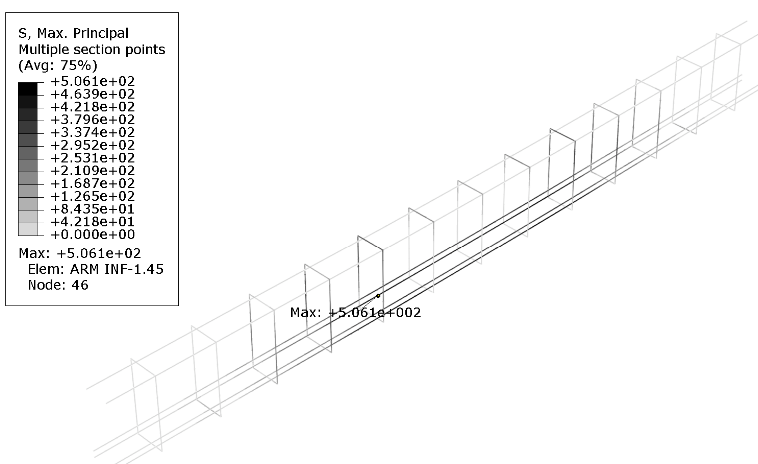

Figure 14—Contour of the stress in the internal steel bars of the FRP strengthened RC beam.

Shear strength of FRP reinforced concrete beams without stirrups: verification of fracture mechanics formulation

Fabio Matta[1], Paolo Mazzoleni[2], Emanuele Zappa[3], Michael A. Sutton[4], Mohamed ElBatanouny[5], Aaron K. Larosche[6], Paul H. Ziehl[7]

[1] *Dept. of Civil and Environ. Engr., University of South Carolina, Columbia, SC, USA, fmatta@sc.edu*
[2] *Dept. of Mechanics, Politecnico di Milano, Milan, Italy, paolo2.mazzoleni@mail.polimi.it*
[3] *Dept. of Mechanics, Politecnico di Milano, Milan, Italy, emanuele.zappa@mecc.polimi.it*
[4] *Dept. of Mechanical Engineering, University of South Carolina, Columbia, SC, USA, sutton@sc.edu*
[5] *Dept. of Civil and Environ. Engr., University of South Carolina, Columbia, SC, USA, elbatano@email.sc.edu*
[6] *Dept. of Civil and Environ. Engr., University of South Carolina, Columbia, SC, USA, larosche@email.sc.edu*
[7] *Dept. of Civil and Environ. Engr., University of South Carolina, Columbia, SC, USA, ziehl@cec.sc.edu*

SYNOPSIS:
The size effect in shear in reinforced concrete (RC) one-way members without shear reinforcement becomes more of concern when using glass fiber reinforced polymer (GFRP) reinforcement. In fact, the lower axial stiffness of GFRP reinforcement typically results in wider flexural cracks with respect to steel RC counterparts. This issue is especially relevant for the case of flexural members without stirrups, such as retaining walls and slab bridge superstructures. Little evidence has documented the extent of such effect. Cognizant of this knowledge gap, ACI Committee 440 (FRP Reinforcement) introduced the current nominal shear strength algorithm, which was calibrated in a conservative fashion based on test results from small beams. This algorithm assumes that the shear strength at the critical section is resisted predominantly through the uncracked concrete above the tip of the shear crack. Based on the same fundamental assumption, a fracture mechanics algorithm for steel RC beams was recently proposed by ACI Committee 446 (Fracture Mechanics of Concrete). In this paper, the ACI 440 and 446 algorithms are verified and discussed based on experimental evidence from tests on scaled GFRP RC beams without stirrups. The latter algorithm is modified to account for the smaller elastic modulus of GFRP, under the hypothesis that its relevant parameters and the shear failure mechanism are similar irrespective of the reinforcement material.

Keywords: design, fiber-reinforced polymers, fracture mechanics, reinforced concrete, shear, size effect, strength

Fabio Matta, Paolo Mazzoleni, Emanuele Zappa, Michael A. Sutton,
Mohamed ElBatanouny, Aaron K. Larosche, and Paul H. Ziehl

ACI member **Fabio Matta** is an Assistant Professor in the Department of Civil and Environmental Engineering at the University of South Carolina. His research interests include sustainable material systems for the new construction and rehabilitation of concrete structures.

Paolo Mazzoleni is a PhD Student in the Department of Mechanics at the Politecnico di Milano. His research interests include the application of mechanical and thermal measurement techniques to concrete testing.

Emanuele Zappa is an Assistant Professor in the Department of Mechanics at the Politecnico di Milano. His research interests include include the application of mechanical and thermal measurement techniques to concrete testing.

Michael A. Sutton is a Carolina Distinguished Professor in the Department of Mechanical Engineering at the University of South Carolina. His research interests include the application of optical measurement techniques to concrete testing.

ACI member **Mohamed K. ElBatanouny** is a PhD Student in the Department of Civil and Environmental Engineering at the University of South Carolina. His research interests include the monitoring and assessment of concrete structures.

ACI member **Aaron K. Larosche** is a PhD Student in the Department of Civil and Environmental Engineering at the University of South Carolina. His research interests include the monitoring and assessment of concrete structures.

ACI member **Paul H. Ziehl** is an Associate Professor in the Department of Civil and Environmental Engineering at the University of South Carolina. His research interests include load testing, structural monitoring and assessment, and sustainable material systems for concrete structures.

INTRODUCTION

The corrosion resistance of fiber reinforced polymer (FRP) reinforcement has made it an attractive option for structures that operate in aggressive environments, such as bridges, parking garages, retaining walls, seawalls, docks and wharves (Fig. 1)[1]. Glass FRP (GFRP) reinforcement has a higher susceptibility to creep rupture than carbon FRP (CFRP)[2] and is best suited for non-prestressed applications. In addition, the relatively low shear strength and brittleness of GFRP bars are highly desirable properties for "softeye" areas in temporary retaining walls for tunnel excavation, where the penetration of tunnel boring machines is greatly facilitated (Fig. 2), making this technology mainstream[1]. Design principles are fairly well established. In the last 14 years, guideline documents have been published in North America[3,4], Europe[5,6] and Japan[7]. In Canada, the use of FRP reinforcement is codified in Section 16 of the Canadian Highway Bridge Design Code[8], and is transitioning from government-subsidized research projects to projects based on traditional bid letting processes and competitive bidding from multiple FRP bar suppliers. In the US, material and construction specifications were published in 2008 by ACI[9,10], and were followed in 2009 by the design specifications for GFRP RC bridge decks and railings published by AASHTO[11].

Among the unresolved issues in the design of FRP RC structures, the understanding of the mechanisms and implications of size effect on the shear strength of slender beams without shear reinforcement is of fundamental and practical significance. The decrease in strength results primarily from the larger width of the critical shear cracks as the effective depth of the cross section is increased. This effect has been extensively documented for the case of steel reinforced concrete (RC)[12-14]. The shear strength of FRP RC beams without shear reinforcement is smaller than that of steel RC counterparts having flexural reinforcement with a similar cross sectional area[15]. In fact, the lower longitudinal elastic modulus of FRP results in deeper and wider cracks, which may exacerbate the size effect[16].

The existing design algorithms for the nominal shear strength recognize the predominant influence of the axial stiffness of the flexural reinforcement on the shear strength of FRP RC beams. This effect is illustrated in Fig. 3(a), which shows the normalized shear strength (defined as the shear stress at failure divided by $f_c^{0.5}$, where f_c is the concrete cylinder compressive strength) from 81 test results from the literature[17-29] with respect to the effective reinforcement ratio, ρ_{eff} (defined as the FRP reinforcement ratio, ρ_f, multiplied by the ratio of the longitudinal elastic modulus of FRP to that of steel, E_f / E_s[15], which is about 0.2 for GFRP bars).

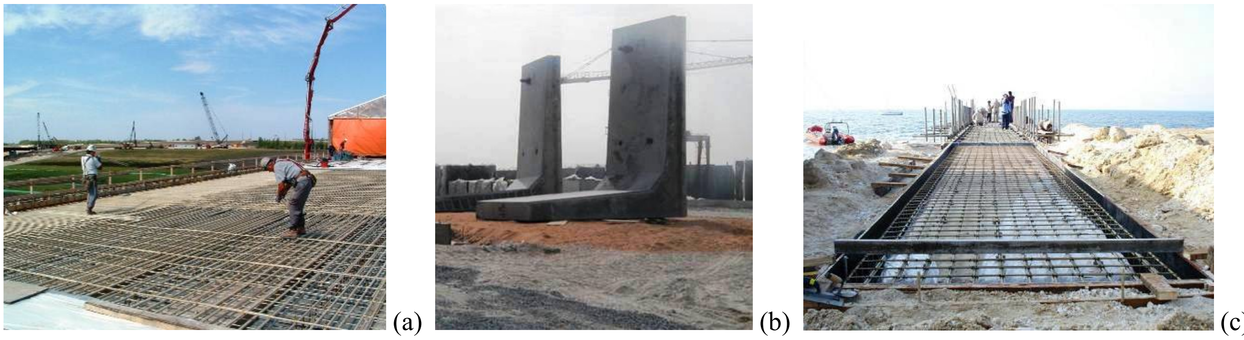

Figure 1—Applications of GFRP reinforcement in concrete for durability: (a) bridge deck (Winnipeg, Manitoba, Canada); (b) precast seawalls (Abu Dhabi, UAE); and (c) marine dock (Dubai, UAE)

Figure 2—Applications of GFRP reinforcement in concrete softeyes: (a) splicing of steel and GFRP softeye cage; (b) erection and installation (Dubai, UAE); and (c) penetration of tunnel boring machine at exit (Portland, OR)

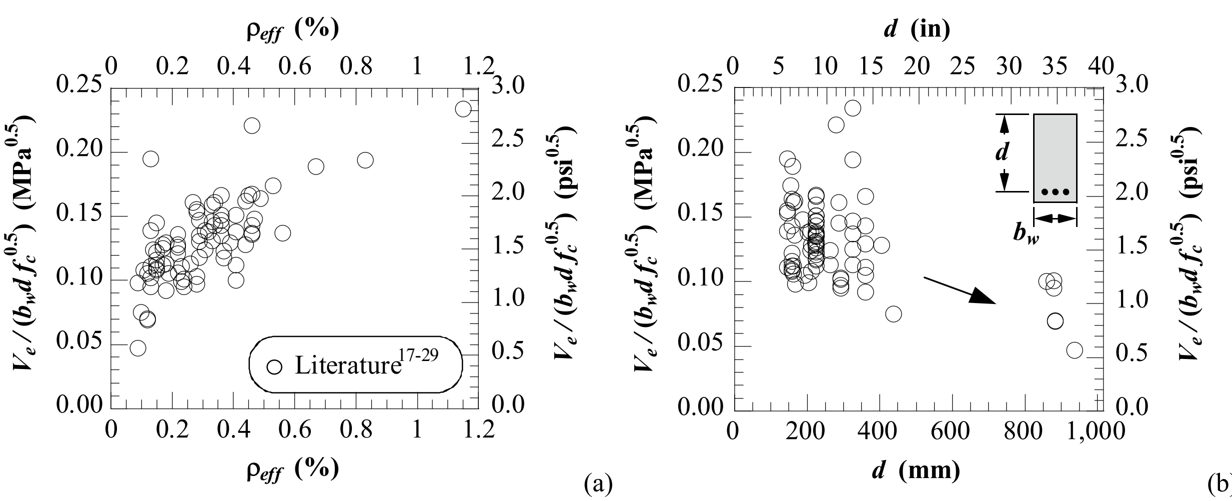

Figure 3—Normalized experimental shear strength of 81 FRP RC beam tests from literature[17-29] with respect to: (a) effective reinforcement ratio, ρ_{eff}, and (b) effective depth, d

However, the existing nominal shear strength algorithms, including that adopted by ACI Committee 440 (Fiber-Reinforced Polymer Reinforcement) in the ACI 440.1R-06 guidelines[3] and by AASHTO in its bridge design specifications[11], have been calibrated and validated on the basis of test results from beam and one-way slab specimens having a maximum effective depth of 360 mm (14.2 in)[15]. This size is not representative of larger scale members that are likely to be considered in practice, such as slab bridge superstructures and large-size retaining walls and seawalls. The significance of the influence of size (effective depth, d) on the shear strength is illustrated in Fig. 3(b), where the normalized shear strength of large-size specimens [$d \geq 850$ mm (33.9 in)] is based on evidence from the only two studies reported in the open literature to date[20,29], to the best of the authors' knowledge.

The current ACI 440 equation[3] is a simplified version of an algorithm[15] that is based on the assumption that the shear force is resisted primarily by the uncracked concrete above the neutral axis at the critical shear crack section. The design algorithm was rendered in a conservative fashion, cognizant of the limited number of results available for calibration purposes, and of the lack of evidence of size effect[15]. Based on the same fundamental assumption, a fracture mechanics algorithm for steel RC was recently proposed by ACI Committee 446 (Fracture Mechanics of Concrete)[30], where the size effect is attributed to the reduced shear capacity of the uncracked concrete above the tip of the critical shear crack subjected to shear-compression fracture[31].

In this paper, the ACI 440[3] and 446[30] algorithms are verified and discussed based on new experimental evidence from tests on scaled GFRP RC beams without stirrups, with respect to effective depth, d, and aggregate size, a_g. The ACI 446 algorithm[30] is herein modified to account for the smaller elastic modulus of GFRP, under the hypothesis that the relevant parameters and the shear failure mechanism are similar irrespective of the reinforcement material.

EXPERIMENTS

Four-point bending tests were performed on five scaled GFRP RC beams without shear reinforcement, all of which were designed to fail in shear (diagonal tension). The specimens included: three small-size beams with d = 146 mm (5.75 in), GS1, GS2 and GS3; and two medium-size beams with d = 292 mm (11.5 in), GM1, GM2 and GM3. The specimens are identified using the format "GXY", where "G" indicates the reinforcement material (GFRP), "X" indicates the size ("S" for small, "M" for medium), and "Y" indicates the specimen number. The evidence obtained from these specimens is complemented by that from recent experiments where similar specimen design and test setups were used, in addition to scaled large-size [d = 883 mm (34.8 in)] counterparts[29].

Specimens

The scaled specimen geometry, test setup geometry and relevant material properties are illustrated in Fig. 4 and Table 1. Specimens GS and S6[29] and their medium-size counterparts GM and S3[29] were designed using Ø16 mm (#5) GFRP bars to attain a ρ_{eff} in the range 0.13-0.15. The ρ_{eff} of 0.15 is similar to the minimum value reported in the literature and that was used to calibrate the ACI 440 algorithm[3], and is a lower bound representative of real-case scenarios. The large-size specimens S1[29] were designed using Ø32 mm (#10) GFRP bars, attaining a ρ_{eff} of 0.12, thus comparable to that of the smaller cross sections.

The beams GS (and S6[29]) and GM (and S3[29]) were designed to scale their effective depth, d, by 1/6 and 1/3 with respect to the S1[29] beams, while maintaining a similar reinforcement ratio using Ø16 mm (#5) GFRP bars. The range for d of 146 mm (5.75 in) to 883 mm (34.8 in) covered by the test matrix in Table 1 significantly extends that used to calibrate the ACI 440 nominal shear strength algorithm[3]. In addition, the scaled beams GS3 (small), GM1 and GM2 (medium), and S1-0.12-1A and S1-0.12-2B[29] (large) were cast using aggregate sizes a_g of 6.3, 12.7 and 19.1 mm (0.25, 0.50 and 0.75 in), respectively, thereby reducing the influence of a_g on shear strength while maintaining realistic maximum aggregate sizes.

Materials

The specimens were constructed using pultruded E-glass/vinyl ester GFRP bars as the flexural reinforcement. The longitudinal elastic modulus, E_f, and the tensile strength, f_{fu}, were characterized per ASTM D7205. The average value of E_f for the flexural reinforcement in each specimen and the associated effective reinforcement ratio, ρ_{eff}, are summarized in Table 1. The specimens were cast using normal weight concrete with maximum aggregate size, a_g, ranging from 6.3 and 19.1 mm (0.25 and 0.75 in), as reported in Table 1. A maximum of six concrete cylinders [with 102 mm (4 in) diameter and 203 mm (8 in) height] were tested for each batch used in accordance with ASTM C39. The mean compressive strength, f_c, for each beam specimen at the day of testing is reported in Table 1.

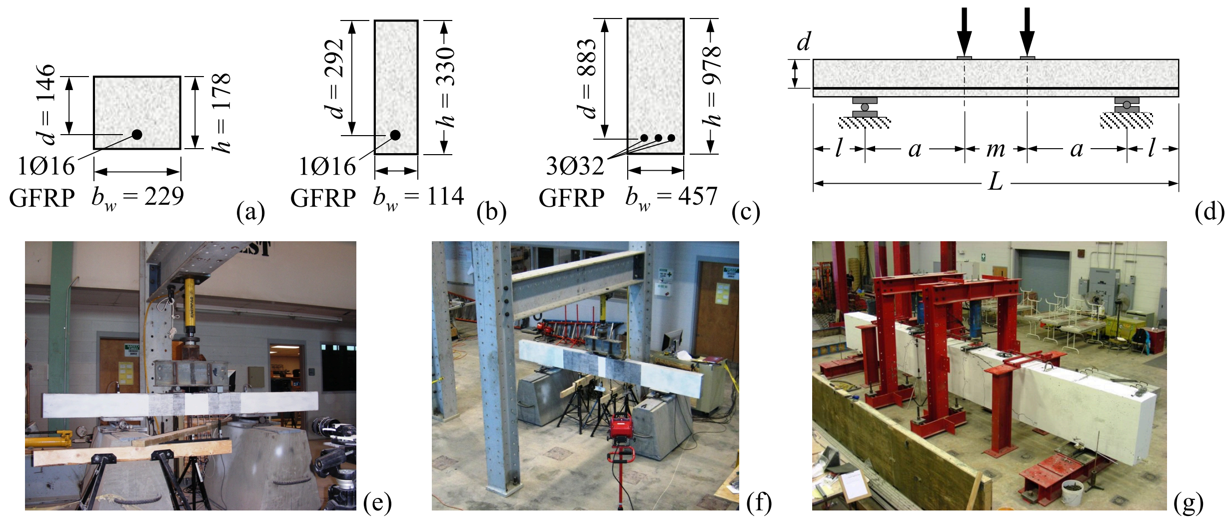

Figure 4—Experimental program: cross section of (a) GS and S6[29], (b) GM and S3[29], and (c) large-size S1 specimens[29]; (d) schematic of test setup; and photograph of setup for (e) GS, (f) GM, and (g) S1-0.12[29] specimens. [Cross sections not to scale. Dimensions in mm (1 mm = 0.0394 in)]

Table 1—Test Matrix: Specimen Geometry and Relevant Material Properties

Specimen ID	b_w [mm (in)]	d [mm (in)]	a [mm (in)]	a/d	m [mm (in)]	l [mm (in)]	f_c [MPa (psi)]	a_g [mm (in)]	E_f [GPa (ksi)]	ρ_{eff} [%]
Small Size										
GS1	229 (9.0)	146 (5.75)	457 (18.0)	3.1	305 (12.0)	610 (24.0)	41.1 (5,957)	12.7 (0.5)	49.3 (7,157)	0.15
GS2							40.8 (5,912)			
GS3							46.8 (6,794)	6.3 (0.25)		
S6-0.12-1A[29]							59.7 (8,652)	19.1 (0.75)	43.2 (6,268)	0.13
S6-0.12-2A[29]							32.1 (4,660)			
S6-0.12-3A[29]										
Medium Size										
GM1	114 (4.5)	292 (11.5)	914 (36.0)	3.1	305 (12.0)	610 (24.0)	40.1 (5,815)	12.7 (0.5)	49.3 (7,157)	0.15
GM2							41.6 (6,035)			
S3-0.12-1A[29]							32.1 (4,660)	19.1 (0.75)	43.2 (6,268)	0.13
S3-0.12-2A[29]										
Large Size										
S1-0.12-1A[29]	457 (18.0)	883 (34.8)	2,743 (108)	3.1	1,829 (72.0)	914 (36.0)	29.5 (4,276)	19.1 (0.75)	41.0 (5,946)	0.12
S1-0.12-2B[29]							29.6 (4,293)			

Test setup and instrumentation

The four-point bending load test setup used is illustrated in Fig. 4. Table 1 summarizes the length of the shear span, *a*, the length of the constant moment region, *m*, and the anchorage length past the supports, *l*, for the straight bar ends. A constant shear span-to-depth ratio, *a*/*d*, of 3.1 was ensured for all specimens to minimize arching action, and yield conservative values of shear strength[12]. The loads were applied using hydraulic actuators and measured with load cells. The specimens were instrumented with strain gauges to measure deformations in the GFRP bars and the concrete, and with displacement transducers to measure vertical deflections.

RESULTS AND DISCUSSION

For all specimens, Table 2 summarizes the experimental shear force at failure, V_e, the normalized shear strength, the theoretical shear force associated with flexural failure, V_b, computed per ACI 440.1R-06[3], and the failure mode. The contribution of self weight computed at a distance d from the loading section is accounted for in Table 2, assuming a concrete density of 2,320 kg/m^3 (145 lb/ft^3).